High-order solutions of three-dimensional rough-surface scattering problems at high frequencies. I: the scalar case

Fernando Reitich and Catalin Turc

School of Mathematics, University of Minnesota, Minneapolis, 55455, USA

E-mail: reitich@math.umn.edu, turc@math.umn.edu

Abstract. We present a new high-order numerical method for the solution of high-frequency scattering problems from rough surfaces in three dimensions. The method is based on the asymptotic solution of appropriate integral equations in the high-frequency regime, in a manner that bypasses the need to resolve the fields on the scale of the wavelength of radiation. Indeed, inspired by prior work in two dimensions, we seek a solution of the integral equation in the form of a slow modulation of the incoming radiation, and we choose a series expansion in inverse powers of the wavenumber to represent the unknown slowly varying envelope. As we show, this framework can be made to yield an efficiently computable recursion for the terms in the series to any arbitrary order. The resulting algorithms generally provide a very significant improvement over classical (e.g. Kirchhoff's) approximations in both accuracy and applicability and they can, in fact, effectively produce results with full double-precision accuracy for configurations of practical interest and up to the resonance regime.

Submitted to: *Waves Random Media*

1. Introduction

The prediction of electromagnetic and acoustic scattering from rough surfaces is at the core of a variety of technologies ranging from SAR imaging and remote sensing [1] to underwater acoustics [2], optical lithography [3] and metrology. The design of numerical algorithms that can be used to faithfully and efficiently simulate scattering processes, and thus be trusted to guide further advances in these and other engineering/industrial applications, however, presents significant challenges. These challenges are largely due to the need of classical numerical methods to resolve wave oscillations and the interactions of these with possibly complex structures, needs these that can quickly translate into prohibitive computational times [4]. Moreover, these limitations are further exacerbated by accuracy requirements that may arise in practice and which can demand highly precise solutions (up to 10 digits) to uncover significant phenomena [5].

As a result of the inordinate expense associated with the use of rigorous numerical methods to accurately resolve full-wave models at high frequencies, state-of-the-art simulation methodologies rely, in these cases, on the solution of approximate, asymptotic models, most notably those based on the Kirchhoff approximation (KA) [9]. Indeed, KA has been extensively used in rough-surface scattering modeling [6, 7, 8, 9] and its applicability has been thoroughly investigated. These studies, in turn, prompted a variety of efforts to derive next-order corrections (in wavelength) in attempts at extending its domain of validity (see e.g. [10, 11, 12, 13] and the references cited therein). At finite frequencies, however, these approximations incur in sizeable errors (see §4.2) that may render them inadequate for certain applications. As these are generally low-order theories (based on low-order approximations to the full wave model) no mechanism is available to improve on the quality of the predictions. A notable exception is the recent work of Bruno et al. [14]. There the authors introduce an algorithm to produce corrections to KA of *arbitrarily high order* in two-dimensional rough-surface scattering configurations, and they show that such corrections can be used to produce very accurate results in this context. In this paper, we present a significant extension of this approach to the simulation of (scalar) wave scattering off *fully three-dimensional* structures, and we demonstrate that results of analogous quality can be garnered through the use of high-order versions of this procedure.

Our approach, following [14], is based on a direct evaluation of the terms in a (Luneburg-Kline) expansion of a surface potential (the normal velocity in acoustics) satisfying an integral equation formulation of the scattering problem. More precisely, we shall seek this unknown potential in the form of a series in inverse powers of the wavenumber modulated by the incoming radiation. Within this framework, we show that the successive terms in the series can be determined, to any desired order, through an *explicit*, computable recurrence (which at lowest order coincides with KA). As in [14] the basic mathematical derivations are based on the analytic evaluation of oscillatory integrals. However, significant differences and new challenges arise in treating fully three-dimensional structures, which are largely

due to the substantially different behavior of the corresponding kernels in the integral formulation (related to the free-space Green's function) and, of course, to the increased dimensionality. As we show below (§3), these issues can be successfully resolved by appealing to appropriate changes of variables and series expansions which, as we mentioned, can be pursued to arbitrarily high orders. Indeed, as we demonstrate (§4.2), the high-order nature of the method translates into results that can display machine accuracy for configurations of practical interest up to the resonance regime, constituting very significant improvements over those provided by KA or its low-order extensions.

As we said, the present contribution relates to scalar scattering problems and, as is the case for standard low-order high-frequency approximations (e.g. KA), it is restricted to configurations that preclude shadowing effects (here, as we show below —see (26)–, this latter condition arises naturally on evaluation of the relevant oscillatory integrals). Future work will address extensions to the vector electromagnetic case, which can be attained based on the concepts introduced herein. Similarly, extensions to shadowing configurations, possibly based on "geometrical shadowing functions" [15], on fractional asymptotic expansions [16] or on "localized integration" [17] strategies are also left for future consideration.

For the present discussion then, we begin in §2 by introducing the relevant integral formulation which we recast in a manner that is well-suited for high-frequency evaluations. The asymptotic expansions of the terms in this formulation are then presented in §3 where we also use these to derive an explicit recurrence that delivers progressively more accurate approximations to the unknown surface potential. A numerical procedure based on this recursion is detailed in §4.1 and numerical results are presented in §4.2. Finally, our conclusions are summarized in §5.

2. High-frequency integral equations

We consider the problem of scattering of time harmonic acoustic waves from an impenetrable surface $\Sigma = \{z = f(x,y) \,:\, (x,y) \in \mathbb{R}^2\}$ where f is a smooth function of the variables (x,y). For the sake of definiteness we shall assume that the surface Σ is "sound soft" though, as will be clear from the discussion that follows, our developments can be easily adapted to other boundary conditions. With this choice then we seek to solve the scattering problem

$$\begin{aligned} &\Delta u + k^2 u = 0 \quad \text{in } \Sigma_+, \\ &u = -u^{\text{inc}} \qquad \text{on } \Sigma \end{aligned} \tag{1}$$

for the scattered field u, where

$$\Sigma_+ = \{\mathbf{r} = (x,y,z) \,:\, z > f(x,y)\}$$

and the incidence is given by

$$u^{\text{inc}} = \exp\left(i\mathbf{k}\cdot\mathbf{r}\right) = \exp\left[i\left(\alpha x + \beta y - \gamma z\right)\right]$$

with

$$\mathbf{k} = (\alpha, \beta, -\gamma)$$

and

$$\alpha = k \sin\psi \cos\phi,\ \beta = k \sin\psi \sin\phi,\ \gamma = k \cos\psi,\ k = |\mathbf{k}|.$$

To define the physically realizable solution of problem (1) this must be supplemented with appropriate "radiation conditions" at infinity. In the case of bi-periodic surfaces, these conditions take on a simple form in terms of the Rayleigh series [18] (see §4.1) while in general they can be cast, for instance, in terms of "upward propagating" potentials [19].

As we anticipated, our method of solution is based on an integral equation formulation of (1). A variety of such formulations can be derived via a direct or indirect use of Green's identities, leading to integral equations of the first or second kind. Interestingly, for the developments that follow the specific choice of integral formulation is immaterial (though it *can* matter if the method we propose below is extended iteratively to account for multiple scattering; see [17]). For the sake of brevity, here we shall only present our derivations as they apply to the classical formulation [20]

$$\frac{1}{2}\eta(\mathbf{r}, k) + \int_\Sigma \frac{\partial G_k(\mathbf{r} - \mathbf{r}')}{\partial \mathbf{n}(\mathbf{r})} \eta(\mathbf{r}', k)\, d\sigma(\mathbf{r}') = \frac{\partial u^{\mathrm{inc}}(\mathbf{r})}{\partial \mathbf{n}(\mathbf{r})}, \quad \mathbf{r} \in \Sigma. \tag{2}$$

wherein the unknown surface potential $\eta(\mathbf{r})$ coincides with a physical quantity

$$\eta(\mathbf{r}, k) = \frac{\partial u(\mathbf{r})}{\partial \mathbf{n}(\mathbf{r})}$$

and

$$G_k(\mathbf{r}) = \frac{\exp(ik|\mathbf{r}|)}{4\pi|\mathbf{r}|}$$

denotes the free-space Green's function; the corresponding derivations based on alternative integral equations are entirely analogous.

In the high-frequency regime, $k \gg 1$, the difficulties associated with the solution of (2) are exacerbated by the highly oscillatory nature of *both* the Green's function and the surface potential. As is well-known, however, the oscillations in the latter can be identified *a-priori* through asymptotic techniques. Indeed, in general, the geometrical optics approximation (see e.g. [16]) guarantees that, asymptotically,

$$\eta(\mathbf{r}, k) = \frac{\partial u(\mathbf{r})}{\partial \mathbf{n}(\mathbf{r})} = \exp(ikS(\mathbf{r}))\, \eta_{\mathrm{slow}}(\mathbf{r}, k)$$

where the phase S satisfies the eikonal equation. In the most general case this phase will be multi-valued, corresponding to multiple-scattering configurations. In the context of approximate high-frequency methods for the solution of (2) (such as KA and its extensions) these multiple reflections can be dealt with iteratively [11, 21] once the technique is rendered applicable to single-scattering cases (as is the case with the aforementioned approximations).

In these latter instances, on the other hand, the phase S is simply that of the incoming radiation [22], that is

$$\eta(\mathbf{r},k)=\frac{\partial u(\mathbf{r})}{\partial \mathbf{n}(\mathbf{r})}=\exp\left(i\mathbf{k}\cdot\mathbf{r}\right)\eta_{\text{slow}}(\mathbf{r},k). \tag{3}$$

The representation (3) has been extensively used in the design of (low-order) analytical scattering theories (see e.g. [10, 13, 23, 24, 25, 26] and the references therein), and it is the form we shall assume for the derivation of our new solution procedure below.

Indeed, within our context, the use of relation (3) reduces the problem of finding η in (2) to that of identifying the envelope η_{slow} which satisfies

$$\frac{1}{2}\eta_{\text{slow}}(\mathbf{r},k)+\int_{\Sigma}\frac{\partial G_k(\mathbf{r}-\mathbf{r}')}{\partial \mathbf{n}(\mathbf{r})}\exp\left[i\mathbf{k}\cdot(\mathbf{r}'-\mathbf{r})\right]\eta_{\text{slow}}(\mathbf{r}',k)\,d\sigma(\mathbf{r}')=u^{\text{inc}}_{\text{slow}}(\mathbf{r},k),\quad \mathbf{r}\in\Sigma \tag{4}$$

where

$$u^{\text{inc}}_{\text{slow}}(\mathbf{r},k)=ik\mathbf{d}\cdot\mathbf{n}(\mathbf{r}).$$

In parametric coordinates, equation (4) can be written as

$$\begin{aligned}\mu(x,y,k)+\frac{1}{2\pi}\int_{\mathbb{R}^2} g(x,y;x',y';k)\exp\left[ikd+i\alpha(x'-x)+i\beta(y'-y)-i\gamma(f(x',y')-f(x,y))\right]\\ \times\mu(x',y',k)dx'dy'=-2ik(f_x(x,y)\sin\psi\cos\phi+f_y(x,y)\sin\psi\cos\phi+\cos\psi)\end{aligned} \tag{5}$$

where we have set

$$\begin{aligned}\mu(x,y,k)&=\eta_{\text{slow}}(x,y,f(x,y);k)\left(1+f_x^2(x,y)+f_y^2(x,y)\right)^{1/2}\\ g(x,y;x',y';k)&=\frac{(x'-x)f_x(x,y)+(y'-y)f_y(x,y)+f(x,y)-f(x',y')}{d^3}(ikd-1)\end{aligned} \tag{6}$$

and

$$d=|\mathbf{r}-\mathbf{r}'|=\left[(x-x')^2+(y-y')^2+(f(x,y)-f(x',y'))^2\right]^{1/2}.$$

Equation (5) possesses two significant advantages over the original formulation (2). First, the new unknown is *not* highly oscillatory and thus it can be represented with relatively few degrees of freedom; in particular, the slowly oscillatory character of $\mu(x,y,k)$ allows for a representation

$$\mu(x,y,k)=\sum_{n=-1}^{\infty}\mu_n(x,y)k^{-n}. \tag{7}$$

On the other hand, while the unknown in (5) can be coarsely discretized, the kernel in this equation remains as highly oscillatory as that of the original equation (2) and thus, in principle, the evaluation of the corresponding integrals entails similar computational costs. Here, however, is where the second advantage of (5) over (2) manifests itself. Indeed, the extraction of the oscillatory part of the unknown potential that delivered (5) additionally implies that the full phase of the integrand in this formulation is now *known*. And this,

in turn, opens the possibility for *explicit* evaluations through classical techniques for the asymptotic expansion of oscillatory integrals [27]. More precisely, substituting (7) into (5) we obtain

$$\sum_{n=-1}^{\infty} k^{-n} \left(\mu_n(x,y) + \frac{1}{2\pi} I^n(x,y,k) \right) = -2ik(f_x(x,y)\sin\psi\cos\phi + f_y(x,y)\sin\psi\cos\phi + \cos\psi) \tag{8}$$

where

$$I^n(x,y,k) = \int_{\mathbb{R}^2} g(x,y;x',y';k) \exp\left[ikd + i\alpha(x'-x) + i\beta(y'-y) - i\gamma(f(x',y') - f(x,y))\right] \mu_n(x',y')\, dx'dy'. \tag{9}$$

As we show below, the expansion in inverse powers of the wavenumber k of the integrals I^n in (9) can be found analytically leading, through (8), to an explicit recurrence for μ_n, which will serve as the basis for our numerical scheme.

3. Asymptotic expansions and the recurrence

As we stated, to derive an asymptotic expansion for the integrals in (9) we shall resort to the general theory of oscillatory integrals, that is, of integrals of the form

$$I = \int_{\mathcal{D}} \exp\left(ik\psi(\mathbf{r}')\right) h(\mathbf{r}')\, d\mathbf{r}'. \tag{10}$$

We recall that the basic observation in this theory relates to the identification of the main contribution to such integrals as arising (asymptotically, as $k \to \infty$) from *critical points* [27]. In general, these points correspond to all points on the boundary of the integration domain, and all points inside the domain where either the *phase* (ψ in (10)) is *stationary* or where the integrand is *singular*. In our case, the integration domain consists of all of $\mathbb{R}^2$ so that there are no boundary contributions. In addition, in the absence of shadowing, it can be easily shown that the phase in (9) is nowhere stationary. Thus, we need only consider contributions to $I^n(x,y,k)$ that arise from the singularity of the integrand at the "target point" $(x,y,f(x,y))$ (cf. (6)).

To explicitly compute the value of the integral $I^n(x,y,k)$ in terms of the contributions that arise from the corresponding target point, we begin by introducing a change of variables that takes advantage of the specific form of the three-dimensional Green's function to reduce the asymptotic evaluation of the singular integral to that of one with a regular integrand. The change of variables is a simple mapping to polar coordinates centered at the target point

$$x' = x + \rho\cos\theta,\ \ y' = y + \rho\sin\theta$$

which transforms the integral to

$$I^n(x,y,k) = ik\int_0^{2\pi} d\theta \int_0^{\infty} d\rho \exp\left[ik\Phi(x,y,\theta,\rho)\right] F^n(x,y,\theta,\rho) - \\ - \int_0^{2\pi} d\theta \int_0^{\infty} d\rho \exp\left[ik\Phi(x,y,\theta,\rho)\right] G^n(x,y,\theta,\rho) \tag{11}$$

where

$$\begin{aligned}\Phi(x,y,\theta,\rho) &= \rho\sin\theta\sin\psi\sin\phi - \cos\psi(f(x+\rho\cos\theta, y+\rho\sin\theta) - f(x,y)) \\ &+ \rho\cos\theta\sin\psi\cos\phi + \left(\rho^2 + (f(x+\rho\cos\theta, y+\rho\sin\theta) - f(x,y))^2\right)^{1/2} \\ F^n(x,y,\theta,\rho) &= \rho\frac{\rho\cos\theta f_x(x,y) + \rho\sin\theta f_y(x,y) + f(x,y) - f(x+\rho\cos\theta, y+\rho\sin\theta)}{\rho^2 + (f(x+\rho\cos\theta, y+\rho\sin\theta) - f(x,y))^2} \\ &\times \mu_n(x+\rho\cos\theta, y+\rho\sin\theta)\end{aligned} \tag{12}$$

and

$$\begin{aligned}G^n(x,y,\theta,\rho) &= \rho\frac{\rho\cos\theta f_x(x,y) + \rho\sin\theta f_y(x,y) + f(x,y) - f(x+\rho\cos\theta, y+\rho\sin\theta)}{(\rho^2 + (f(x+\rho\cos\theta, y+\rho\sin\theta) - f(x,y))^2)^{3/2}} \\ &\times \mu_n(x+\rho\cos\theta, y+\rho\sin\theta).\end{aligned} \tag{13}$$

As can be readily verified, the functions F^n and G^n in (12), (13) are smooth functions of (θ,ρ). It then follows that the only critical point in the integral (11) corresponds to the boundary point $\rho = 0$. To evaluate the integral then we proceed to expand F^n, G^n in series in powers of ρ [27]

$$F^n(x,y,\theta,\rho) = \sum_{m=1}^{\infty} p_{n,m}(x,y,\theta)\rho^m \tag{14}$$

and

$$G^n(x,y,\theta,\rho) = \sum_{m=0}^{\infty} q_{n,m}(x,y,\theta)\rho^m, \tag{15}$$

where we have used

$$p_{n,0}(x,y,\theta) = \lim_{\rho\to 0} F^n(x,y,\theta,\rho) = 0$$

as it follows from (12); similarly,

$$\Phi(x,y,\theta,\rho) = \Phi_1(x,y,\theta)\rho + \sum_{j=2}^{\infty} \Phi_j(x,y,\theta)\rho^j \tag{16}$$

where

$$\begin{aligned}\Phi_1(x,y,\theta) &= \sin\theta\sin\psi\sin\phi + \cos\theta\sin\psi\cos\phi \\ &- \cos\psi(f_x(x,y)\cos\theta + f_y(x,y)\sin\theta) + \left(1 + (f_x(x,y)\cos\theta + f_y(x,y)\sin\theta)^2\right)^{1/2}.\end{aligned} \tag{17}$$

Then, using (14), (15) and (16) in (11), we obtain

$$\begin{aligned} I^n(x,y,k) \qquad &= ik\sum_{m=1}^{\infty}\int_0^{2\pi} p_{n,m}(x,y,\theta)d\theta\int_0^{\infty} e^{ik\rho\Phi_1(x,y,\theta)}[e^{ik(\Phi(x,y,\theta,\rho)-\rho\Phi_1(x,y,\theta))}\rho^m]d\rho - \\ &- \sum_{m=0}^{\infty}\int_0^{2\pi} q_{n,m}(x,y,\theta)d\theta\int_0^{\infty} e^{ik\rho\Phi_1(x,y,\theta)}[e^{ik(\Phi(x,y,\theta,\rho)-\rho\Phi_1(x,y,\theta))}\rho^m]d\rho. \end{aligned} \tag{18}$$

Next, we expand the exponential in the bracketed expressions in the right-hand side of (18)

$$\begin{aligned} e^{ik(\Phi(x,y,\theta,\rho)-\Phi_1(x,y,\theta)\rho)} &= 1+\sum_{l\geq 1}\frac{(k\rho)^l}{l!}\left(i\sum_{j\geq 1}\Phi_{j+1}(x,y,\theta)\rho^j\right)^l \\ &= 1+\sum_{l\geq 1}\frac{(k\rho)^l}{l!}\left(\sum_{j\geq l}a_{l,j}(x,y,\theta)\rho^j\right) \end{aligned} \tag{19}$$

where the $a_{l,j}(x,y,\theta)$ are defined by

$$\left(i\sum_{j\geq 1}\Phi_{j+1}(x,y,\theta)\rho^j\right)^l = \sum_{j\geq l}a_{l,j}(x,y,\theta)\rho^j \tag{20}$$

and can be found from the Φ_j by induction in l. Using (19) and introducing an additional change of variables

$$t = k\rho$$

equation (18) can be written as

$$\begin{aligned} I^n(x,y,k) = ik\sum_{m=1}^{\infty}\int_0^{2\pi} p_{n,m}(x,y,\theta)d\theta\int_0^{\infty} e^{it\Phi_1(x,y,\theta)}\sum_{l\geq 0}\frac{t^l}{l!}\sum_{j\geq l}a_{l,j}(x,y,\theta)t^{j+m}k^{-j-m-1}\,dt \\ -\sum_{m=0}^{\infty}\int_0^{2\pi} q_{n,m}(x,y,\theta)d\theta\int_0^{\infty} e^{it\Phi_1(x,y,\theta)}\sum_{l\geq 0}\frac{t^l}{l!}\sum_{j\geq l}a_{l,j}(x,y,\theta)t^{j+m}k^{-j-m-1}\,dt \end{aligned}$$

or, equivalently,

$$\begin{aligned} I^n(x,y,k) = ik\sum_{m=1}^{\infty}\int_0^{2\pi} p_{n,m}(x,y,\theta)d\theta\int_0^{\infty} e^{it\Phi_1(x,y,\theta)}\sum_{j\geq 0}k^{-j-m-1}\sum_{l=0}^{j}a_{l,j}(x,y,\theta)\frac{t^{l+j+m}}{l!}\,dt \\ -\sum_{m=0}^{\infty}\int_0^{2\pi} q_{n,m}(x,y,\theta)d\theta\int_0^{\infty} e^{it\Phi_1(x,y,\theta)}\sum_{j\geq 0}k^{-j-m-1}\sum_{l=0}^{j}a_{l,j}(x,y,\theta)\frac{t^{l+j+m}}{l!}\,dt. \end{aligned} \tag{21}$$

Finally, rearranging the sums in (21) we obtain the asymptotic expansion

$$I^n(x,y,k) = \sum_{r=1}^{\infty} I_r^n(x,y)k^{-r} \tag{22}$$

where

$$I_r^n(x,y) = \sum_{s=0}^{r-1} \int_0^{2\pi} (i\, p_{n,r-s}(x,y,\theta) A_s(r-s,x,y,\theta) - q_{n,r-1-s}(x,y,\theta) A_s(r-1-s,x,y,\theta))\, d\theta\,, \tag{23}$$

$$A_0(r,x,y,\theta) = \int_0^\infty e^{i\Phi_1(x,y,\theta)t} t^r\, dt \tag{24}$$

and

$$A_s(r,x,y,\theta) = \sum_{l=0}^{s} \frac{a_{l,s}(x,y,\theta)}{l!} A_0(r+s+l,x,y,\theta). \tag{25}$$

The definition of the function A_0 (and, consequently, that of A_s) deserves a comment since, as it is clear, the integral in (24) is not convergent. The main observation here is that, within the context of asymptotic expansions, such integrals can (and should) be defined to give a finite value *provided* their integrands are indeed oscillatory. In the case of the integral in (24) this translates into the condition that the phase not vanish, that is

$$\Phi_1(x,y,\theta) \neq 0 \quad \text{for all } (x,y,\theta). \tag{26}$$

As we anticipated, the condition (26) can be easily shown to coincide with the requirement that the configuration does not exhibit shadowing effects. In this case, A_0 can be explicitly found from the Mellin transform pair [27]

$$\int_0^\infty e^{it} t^{z-1}\, dt = e^{\frac{i\pi z}{2}} \Gamma(z) \quad \text{if } 0 < \Re z < 1$$

by analytic continuation. Indeed, we have

$$\begin{aligned} A_0(r,x,y,\theta) &= (\Phi_1(x,y,\theta))^{-r-1} \int_0^\infty e^{iv} v^r dv = (\Phi_1(x,y,\theta))^{-r-1} e^{\frac{i\pi(r+1)}{2}} \Gamma(r+1) \\ &= \frac{r!\, e^{\frac{i\pi(r+1)}{2}}}{(\Phi_1(x,y,\theta))^{r+1}}. \end{aligned} \tag{27}$$

To derive the final recurrence we first note that from equation (22) it readily follows that

$$I^n(x,y,k) = O\left(\frac{1}{k}\right) \quad \text{as } k \to \infty. \tag{28}$$

On the other hand, with regards to the unknown coefficients μ_l, $l = -1, 0, \cdots$, and as is clear from (12)-(15), the integral $I^n(x,y,k)$ depends *only* on $\mu_n(x,y)$ (i.e. $l = n$) and its partial derivatives. Combining this with (28) it follows that equation (8) can be used to recursively find these coefficients. More precisely, from (8) and (23) we have, equating like powers of k,

$$\mu_{-1}(x,y) = -2i(f_x(x,y)\sin\psi\cos\phi + f_y(x,y)\sin\psi\cos\phi + \cos\psi) \tag{29}$$

and

$$\mu_n(x,y) = -\frac{1}{2\pi}\sum_{m=-1}^{n-1} I_{n-m}^m. \tag{30}$$

for $n \geq 0$; note that (29) coincides, of course, with the Kirchhoff approximation [9]. Also, using (23) and (25), equation (30) can be written more explicitly as

$$\begin{aligned}\mu_n(x,y) = -\frac{1}{2\pi}\sum_{m=-1}^{n-1}\sum_{s=0}^{n-m-1}\sum_{l=0}^{s}\int_0^{2\pi}\frac{a_{l,s}(x,y,\theta)}{l!}\Big(i\,p_{m,n-m-s}(x,y,\theta)A_0(n-m+l,x,y,\theta)\\ -q_{m,n-m-s-1}(x,y,\theta)A_0(n-m+l-1,x,y,\theta)\Big)\,d\theta.\end{aligned} \tag{31}$$

4. Numerical Experiments

4.1. Numerical implementation

In this section we describe our numerical implementation of the recurrence (29)-(31). Due to their wide applicability [18], we shall concentrate on the case of doubly periodic surfaces; clearly, the changes necessary for an implementation of more general configurations reduce to choosing an appropriate finite-dimensional representation of the unknowns. In the case of bi-periodic structures with periods d_1 and d_2 the (slow) surface potential is itself periodic, and we shall seek to recursively define $\mu_n(x,y)$, through (29)-(31), on an equispaced Cartesian grid (x_i, y_j) where $1 \leq i \leq N_x$ and $1 \leq j \leq N_y$.

Our implementation is largely based on an extension of that described in [14] to three dimensional geometries. In particular, the overall simulation is divided into "pre-processing", "processing" and "post-processing" stages as follows

- *Pre-processing:* This stage is devoted to the precomputation of all quantities that depend only upon the geometry and incidence. These include the coefficients $\Phi_j(x,y,\theta)$ and $a_{l,s}(x,y,\theta)$ defined in (16) and (20), the integrals $A_0(p,x,y,\theta)$ in (27) and the factors in the definition of $p_{n,m}(x,y,\theta)$ and $q_{n,m}(x,y,\theta)$ (cf. (12)-(15)) that are independent of μ_n. All of these quantities are smooth and periodic functions of θ; thus, they admit rapidly convergent Fourier series expansions whose truncation we use for their numerical representation at each point (x_i, y_j). As is clear from their definition, the actual determination of these Fourier representations entails operations (sums, products, algebraic inverses, square roots) on "Taylor-Fourier series", that is, on expressions of the form

$$H(\rho,\theta) = \sum_{n=0}^{\infty} H_n(\theta)\rho^n = \sum_{n=0}^{\infty}\sum_{m=-\infty}^{\infty} H_{n,m}e^{im\theta}\rho^n. \tag{32}$$

  These manipulations are done using a combination of discrete and fast Fourier transforms, following the prescriptions of [14] to minimize ill-conditioning; similar

considerations apply to the evaluation of composite functions of the form

$$f(x+\rho\cos\theta, y+\rho\sin\theta) \tag{33}$$

whose Taylor-Fourier series must be retrieved solely from knowledge of the values of f at the points (x_i, y_j).

- *Processing:* This is the core of the scheme and where the recurrence (29)-(31) is actually implemented. Again here the evaluation of the coefficients $p_{m,s}$, $q_{m,s}$ demands operations on Taylor-Fourier series (32) as well as expansions of composite functions as in (33) (with f replaced by μ_m).
- *Post-processing:* The final stage is devoted to retrieving any desired information on the fields from knowledge of the surface potential. In particular, we compute far-field data which, in the context of bi-periodic surfaces, can be equated to the amplitudes of the (finitely many) reflected propagating waves. More precisely, the periodicity of the structure implies the quasi-periodicity of the field which, in turn, translates into a representation [18]

$$u(x,y,z) = \sum_{r=-\infty}^{\infty}\sum_{s=-\infty}^{\infty} B_{r,s}\exp(i\alpha_r x + i\beta_s y + i\gamma_{r,s} z)\,, \quad z > \max f(x,y)\,, \tag{34}$$

in the form of a Rayleigh (Fourier) series for the scattered field. Here

$$\alpha_r = \alpha + \frac{2\pi r}{d_1}, \quad \beta_s = \beta + \frac{2\pi s}{d_2}, \quad \text{and} \quad \gamma_{r,s} = \left(k^2 - \alpha_r^2 - \beta_s^2\right)^{1/2} \tag{35}$$

where the last square root is chosen so that $\Im(\gamma_{r,s}) \geq 0$; the propagating modes correspond to the indices in the set $U = \{(r,s) : \Im(\gamma_{r,s}) = 0\}$. On the other hand, in terms of the computed potential, the scattered field admits a representation

$$\begin{aligned} u(x,y,z) = -\int_{\mathbb{R}^2} & G_k\left(x-x', y-y', z-f(x',y')\right) \\ & \times \exp\left(i\alpha x' + i\beta y' - i\gamma f(x',y')\right)\mu(x',y',k)\,dx'\,dy' \end{aligned}$$

or, using the periodized Green's function G_k^{per},

$$\begin{aligned} u(x,y,z) = -\int_0^{d_1}\int_0^{d_2} & G_k^{\mathrm{per}}\left(x-x', y-y', z-f(x',y')\right) \\ & \times \exp\left(i\alpha x' + i\beta y' - i\gamma f(x',y')\right)\mu(x',y',k)\,dx'\,dy'. \end{aligned} \tag{36}$$

We recall [18] that the periodized Green's function

$$G_k^{\mathrm{per}}(x,y,z) = \frac{1}{4\pi}\sum_{r=-\infty}^{\infty}\sum_{s=-\infty}^{\infty} e^{-i\alpha r d_1} e^{-i\beta s d_2} G_k(x+rd_1, y+sd_2, z)$$

can also be expressed as

$$G_k^{\mathrm{per}}(x,y,z) = \frac{i}{2d_1 d_2}\sum_{r=-\infty}^{\infty}\sum_{s=-\infty}^{\infty}\frac{1}{\gamma_{r,s}} e^{i\alpha_r x + i\beta_s y + i\gamma_{r,s}|z|}. \tag{37}$$

Combining (34), (36) and (37) it follows that

$$B_{r,s} = -\frac{i}{2d_1 d_2 \gamma_{r,s}} \int_0^{d_1} \int_0^{d_2} e^{-i\frac{2\pi r}{d_1}x' - i\frac{2\pi s}{d_2}y' - i(\gamma+\gamma_{r,s})f(x',y')} \mu(x', y', k)\, dx'\, dy'$$

which we evaluate in the post-processing stage. In addition, letting

$$e_{r,s} = \frac{|B_{r,s}|^2 \gamma_{r,s}}{\gamma_{0,0}}$$

denote the efficiency at order (r, s), we evaluate the "energy defect"

$$\epsilon = \left| 1 - \sum_{(r,s)\in U} e_{r,s} \right|$$

which vanishes for the exact scattered field.

4.2. Numerical results

In this section, we present numerical results obtained from the implementation of the recurrence (29)-(31) for several profiles and incidences. Specifically, we will consider examples for a "bisinusoidal" profile

$$f_1(x, y) = \frac{h}{h_1}(\cos(2\pi x) + \cos(2\pi y)) \tag{38}$$

for a more oscillatory profile

$$f_2(x, y) = \frac{h}{h_2}(\cos(2\pi x) + \cos(4\pi x) + \cos(2\pi y) + \cos(4\pi y)) \tag{39}$$

and, finally, for the rougher (asymmetric) surface

$$f(x, y) = \frac{h}{h_3}(\cos(2\pi x) + \frac{1}{4}\cos(4\pi x) + \frac{1}{10}\sin(10\pi x))(\cos(2\pi y) + \cos(4\pi y)) \tag{40}$$

where $h_1 = 4$, $h_2 \approx 6.24$ and $h_3 \approx 4.29$ are chosen so that the value of h remains indicative of the height of the profile; see Figure 1.

The first set of results, Tables 1–3, relate to scattering experiments for the three profiles above under normal incidence with a wavelength $\lambda = 0.02$ and a comparable height $h = 0.015$. The tables display the relative errors incurred by our approximations, up to order ten, in some representative efficiencies, along with the corresponding energy defects. The "exact" results were computed with an alternative scheme (the "Method of Variation of Boundaries" [28]) that is known to be highly accurate in this "resonance regime" ($h \approx \lambda$). The values of the efficiencies produced by this latter algorithm, and the corresponding energy error, are displayed in the second column of each table; other columns display the deviation from these results of the values produced by the application of our new procedure at different orders (again, to recall, "Order -1" corresponds to KA). For the experiments corresponding to the first two profiles, (38) and (39), the spatial grid of definition of $\mu_n(x, y)$ was taken to

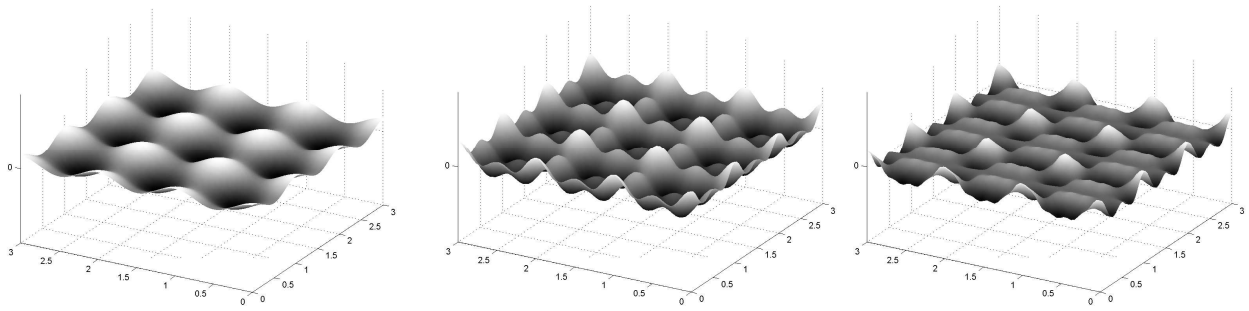

(a) (b) (c)

Figure 1. Plots of an instance of the profiles in (38)–(40) (in (a)–(c) respectively).

Table 1. Results for the profile (38) with $h = 0.015$, $\lambda = 0.02$, $\psi = 0^{\text{o}}$, $\phi = 0^{\text{o}}$.

Efficiency	Scattered energy	Order -1	Order 0	Order 2	Order 4	Order 10
(0,0)	0.4308252680091380e-06	1.92e-02	5.34e-06	2.66e-08	2.50e-11	4.62e-13
(1,0)	0.1857486175897403e-03	9.83e-03	2.59e-06	4.08e-09	4.65e-12	6.62e-14
(1,1)	0.7856829997621104e-01	3.54e-04	1.77e-07	1.57e-10	1.70e-13	0.00e-16
(1,2)	0.5033897260612129e-01	1.20e-05	4.75e-08	6.01e-11	6.57e-14	1.79e-15
(2,2)	0.3218155421621641e-01	3.78e-04	8.30e-08	6.39e-11	6.51e-14	6.46e-16
(2,4)	0.6456288173325015e-03	8.76e-04	9.01e-07	9.44e-10	1.04e-12	4.87e-15
ϵ	1.37e-15	5.55e-08	1.23e-14	1.39e-15	9.01e-16	6.39e-16

Table 2. Results for the profile (39) with $h = 0.015$, $\lambda = 0.02$, $\psi = 0^{\text{o}}$, $\phi = 0^{\text{o}}$.

Efficiency	Scattered energy	Order -1	Order 0	Order 2	Order 4	Order 10
(0,0)	0.1741159809588316e-01	1.03e-03	6.79e-08	1.58e-11	1.42e-13	1.55e-14
(1,0)	0.2189797779360668e-01	9.69e-04	4.69e-07	6.45e-10	3.24e-12	1.33e-14
(1,1)	0.2753679870366883e-01	8.99e-04	8.65e-07	1.22e-09	1.37e-12	5.16e-15
(1,2)	0.1463222323885668e-01	6.18e-04	1.24e-06	3.45e-09	1.31e-11	4.14e-15
(2,2)	0.7783706722436641e-02	3.38e-04	1.62e-06	7.25e-09	2.99e-11	1.51e-14
(2,4)	0.2320249930661595e-02	5.35e-04	2.15e-07	3.03e-09	1.36e-11	1.08e-14
ϵ	1.09e-15	3.87e-07	7.67e-13	2.33e-15	8.94e-16	5.35e-16

be of size $N_x = N_y = 32$ whereas for those pertaining to the more oscillatory profile (40) it was augmented to $N_x = N_y = 64$; in every case, all Taylor-Fourier series of the form (32) were truncated at $n = 10$ and $m = \pm 16$.

Table 3. Results for the profile (40) with $h = 0.015$, $\lambda = 0.02$, $\psi = 0^o$,$\phi = 0^o$.

Efficiency	Scattered energy	Order -1	Order 0	Order 2	Order 4	Order 10
(0,0)	0.1243485673662968e-00	1.04e-03	1.65e-07	1.58e-09	3.02e-12	4.01e-15
(1,0)	0.3050912596549463e-01	7.27e-04	1.47e-06	3.14e-09	2.10e-10	4.68e-14
(1,1)	0.2155272307060579e-01	1.26e-03	1.16e-07	2.07e-09	1.59e-10	3.25e-14
(1,2)	0.1703176206976431e-01	4.07e-04	1.31e-06	1.27e-08	1.73e-10	2.83e-14
(2,2)	0.2190803043377708e-02	3.74e-03	3.50e-06	5.49e-08	7.72e-10	5.80e-14
(2,4)	0.1756411531489210e-05	1.86e-02	8.34e-05	7.66e-07	8.54e-09	3.12e-13
ϵ	2.61e-15	6.04e-07	5.24e-12	3.52e-15	1.16e-15	3.77e-15

We note that, although the tables display the values and errors for selected low-order efficiencies, the calculation must remain accurate for higher-order scattered amplitudes as well in order to retain double-precision accuracy in the energy defect (there are 10201 propagating modes in this case). As we show in Figure 2, this is increasingly relevant with increasing profile roughness which translates in more diffuse energy distributions.

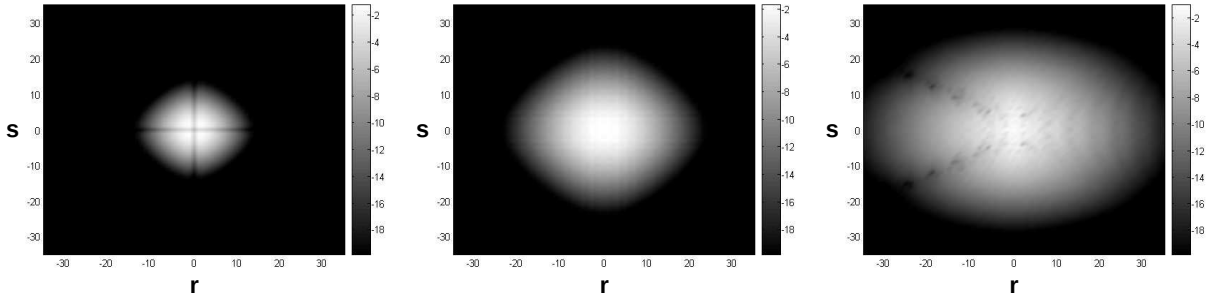

(a) (b) (c)

Figure 2. Plots of calculated energy distribution ($\log_{10}(e_{r,s})$) at order 10 for the examples in Tables 1–3 ((a)–(c), respectively).

The results in Tables 1–3 illustrate the rapid convergence of the overall scheme which, as these examples show, can deliver full double-precision accuracy for configurations up to the resonance regime. In particular, these tables also show that high-order versions of the algorithm can provide very significant improvements over KA at a modest additional cost. We note that, in fact, these rather dramatic improvements are delivered in spite of the lack of exact reciprocity that the method exhibits beyond its lowest order version (i.e. the KA itself). Indeed, while KA is known to be exactly reciprocal (see e.g. [26]), the method we present can be easily seen to deviate from precise reciprocity; see Table 4. The very

Table 4. Relative errors in reciprocity for the example in Table 1.

(r,s)	$\gamma_{r,s}B_{r,s}$	Order -1	Order 0	Order 2	Order 4	Order 10
(1,0)	i 4.281236601628775e+00	1.69e-15	3.96e-08	1.56e-11	2.13e-14	1.03e-15
(1,1)	8.804134267239223e+01	2.26e-17	8.00e-08	2.50e-11	1.32e-14	4.56e-18
(1,2)	-i 7.045059766762202e+01	2.08e-16	2.00e-07	5.91e-11	1.49e-14	1.07e-17
(2,2)	-5.631257507762255e+01	5.08e-16	3.20e-07	9.31e-11	1.80e-14	5.88e-17
(2,4)	7.966530883142464e+00	3.78e-16	8.02e-07	2.32e-10	1.03e-13	5.75e-16

nature of the approach, on the other hand, guarantees that a calculation to order N satisfies the reciprocity relation to that order, that is, with an error of $O(k^{-N-1})$. And this, in turn, implies that this relation can be satisfied to machine accuracy for a sufficiently resolved, high-order approximation. To exemplify these effects, in Table 4 we present the results of such an experiment for the case of Table 1 above (bisinusoidal profile under normal incidence); columns 3 to 7 in this table display the relative errors (deviation from reciprocity)

$$\frac{|\gamma_{r,s}B_{r,s} - \gamma'_{r,s}B'_{r,s}|}{|\gamma_{r,s}B_{r,s}|}$$

where, of course, $\gamma'_{r,s}$ and $B'_{r,s}$ are defined as their corresponding un-primed quantities (cf. (34)-(35)) but with incidence $(-\alpha_r, -\beta_s, -\gamma_{r,s})$.

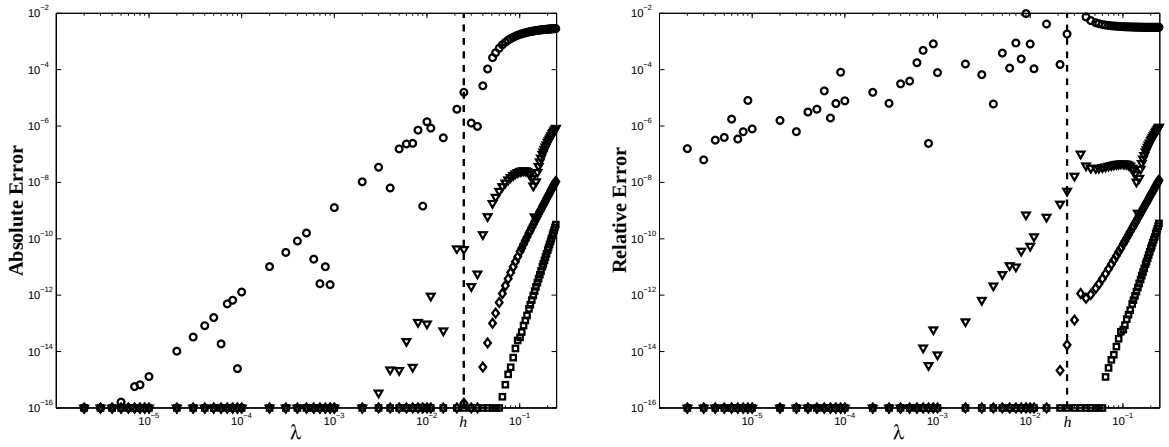

(a) Absolute error

(b) Relative error

Figure 3. Absolute and relative errors in the prediction of the efficiency of order $(0,0)$ for the profile (38) with $h = 0.025$ under normal incidence as a function of the wavelength of radiation. Comparison of results for asymptotic expansions of orders -1 (Kirchhoff, circles), 2 (triangles), 6 (diamonds) and 10 (squares).

The improvements in accuracy as the order of the expansion is increased is further exemplified in Figure 3 where we present the error in the efficiency $e_{0,0}$ as a function of the wavelength of radiation for a configuration of normal incidence on the profile (38) with $h = 0.025$. In these plots the wavelength spans several orders of magnitude, from the very high-frequency ($\lambda = 2 \times 10^{-6}$) to the resonance ($\lambda \approx h$) to the low frequency ($\lambda = 0.25$) regimes. The figures show that double-precision accuracy can be attained throughout this spectrum by increasing the order of the expansion in (7) (here, for short wavelengths, below resonance, the reference solution was taken to be that produced by our new scheme at order 20).

Similar results can be obtained for off-normal illumination. In Tables 5–7, for instance, we present the outcome of our scheme for the case where the incident wavevector is at thirty degrees from vertical; Figure 4 displays the corresponding energy distribution as computed with the 10th order version of our algorithm (in this case, the propagating modes correspond to $-74 \leq r \leq 25$ and $-54 \leq s \leq 45$, and are therefore 10000 in all).

Table 5. Results for the profile (38) with $h = 0.015$, $\lambda = 0.02$, $\psi = 30^{\circ}$, $\phi = 10^{\circ}$.

Efficiency	Scattered energy	Order -1	Order 0	Order 2	Order 4	Order 10
(0,0)	0.1624419003465672e-02	3.62e-03	2.11e-06	1.08e-08	3.97e-11	3.44e-14
(1,0)	0.1439100033360099e-01	1.61e-03	4.66e-06	2.94e-09	1.26e-12	7.23e-16
(1,1)	0.1094401155990229e-00	1.66e-04	4.83e-06	1.95e-09	1.82e-12	2.66e-15
(1,2)	0.4234477682927427e-01	2.51e-04	5.78e-06	2.57e-09	1.56e-12	8.19e-16
(2,2)	0.1577162371639216e-01	8.28e-04	1.16e-05	9.13e-09	9.01e-12	6.59e-16
(2,4)	0.1430959960913712e-03	1.49e-03	1.50e-05	1.36e-08	1.93e-11	2.38e-14
ϵ	1.00e-15	1.02e-07	1.15e-11	5.46e-18	5.70e-16	5.43e-16

Table 6. Results for the profile (39) with $h = 0.015$, $\lambda = 0.02$, $\psi = 30^{\circ}$, $\phi = 10^{\circ}$.

Efficiency	Scattered energy	Order -1	Order 0	Order 2	Order 4	Order 10
(0,0)	0.3255742635101888e-01	2.28e-03	7.64e-07	2.66e-08	3.92e-10	5.49e-14
(1,0)	0.3172711328299686e-01	1.48e-03	1.59e-05	4.87e-08	3.18e-10	1.05e-13
(1,1)	0.2981286890594808e-01	8.35e-04	1.68e-05	3.87e-08	2.45e-10	1.08e-13
(1,2)	0.1968167118759771e-01	2.86e-04	1.90e-05	4.18e-08	2.32e-10	1.04e-13
(2,2)	0.1317696337922965e-01	4.82e-04	3.51e-05	3.88e-08	4.03e-10	1.15e-13
(2,4)	0.2190548455377572e-02	1.70e-03	4.40e-05	6.82e-08	3.38e-10	1.19e-13
ϵ	9.77e-16	7.18e-07	3.16e-10	4.32e-15	8.49e-17	3.47e-16

Table 7. Results for the profile (40) with $h = 0.015$, $\lambda = 0.02$, $\psi = 30^o$, $\phi = 10^o$.

Efficiency	Scattered energy	Order -1	Order 0	Order 2	Order 4	Order 10
(0,0)	0.7804309029307065e-01	7.63e-04	1.05e-05	1.24e-07	2.18e-09	7.78e-12
(1,0)	0.3273439846510247e-01	1.38e-03	2.72e-06	2.04e-08	2.96e-09	1.36e-11
(1,1)	0.1628309817286005e-01	1.00e-03	9.79e-06	1.79e-07	4.54e-09	1.33e-11
(1,2)	0.9897557955011809e-02	7.66e-04	6.78e-07	2.82e-07	5.76e-09	1.13e-11
(2,2)	0.4566940359760414e-02	1.58e-03	4.86e-05	3.37e-07	4.33e-09	1.55e-11
(2,4)	0.2839266200038329e-03	3.00e-03	1.76e-06	1.23e-07	5.85e-09	3.78e-11
ϵ	5.50e-15	6.21e-07	6.84e-10	9.35e-14	6.24e-17	8.01e-16

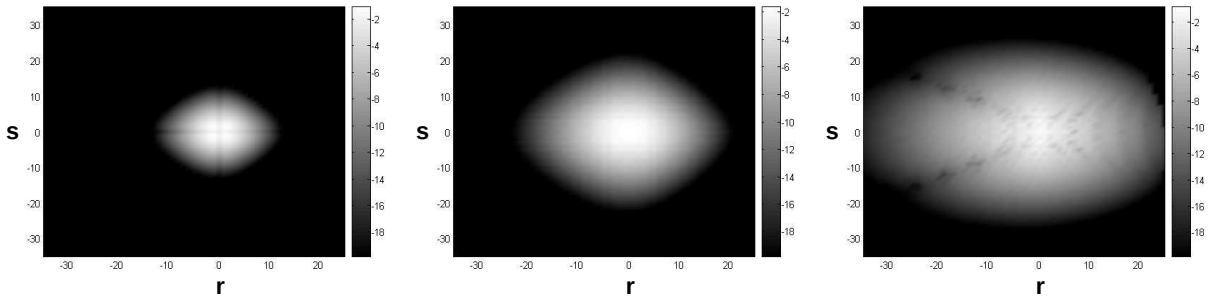

(a) (b) (c)

Figure 4. Plots of calculated energy distribution ($\log_{10}(e_{r,s})$) at order 10 for the examples in Tables 5–7 ((a)–(c), respectively).

We conclude this section with an example that illustrates the behavior of our high-frequency method for near to grazing incidence. In Table 8 we display results corresponding to the profile (38) with $h = 0.01$, $\lambda = 0.0002$ and $\psi = 80^o$ (again here the reference solution was taken to be one produced by a high-order —specifically, tenth order— version of the present method). The corresponding energy distribution is displayed in Figure 5 which shows a significant reduction and a more uniform distribution in the values of the efficiencies. Again here, Table 8 demonstrates the rapid convergence of the scheme.

5. Conclusions

We have presented a scheme for three-dimensional scalar rough-surface scattering simulations that can deliver highly accurate results from low to high frequencies at a cost that is independent of the wavelength. The method is based on *high-order* asymptotic expansions of

Table 8. Results for the profile (38) with $h = 0.01$, $\lambda = 0.0002$, $\psi = 80^{\circ}$, $\phi = 0^{\circ}$.

Efficiency	Scattered energy	Order -1	Order 0	Order 2	Order 4	Order 8
(0,0)	0.1171752315417405e-05	2.81e-03	8.51e-07	4.69e-10	2.96e-13	1.08e-15
(1,0)	0.4585163829816229e-04	1.09e-04	1.31e-06	6.50e-10	1.55e-14	0.00e-00
(1,1)	0.4638341378766691e-03	1.72e-04	1.30e-06	6.49e-10	1.40e-14	0.00e-00
(1,2)	0.2691321057223240e-04	9.06e-05	1.32e-06	6.51e-10	1.66e-14	5.03e-16
(2,2)	0.5614731359279648e-05	1.89e-03	8.24e-07	5.53e-10	2.73e-13	6.03e-16
(2,4)	0.5723728972931240e-06	2.01e-03	6.04e-07	5.25e-10	2.98e-13	1.47e-15
ϵ	1.77e-15	4.64e-08	2.34e-12	1.77e-15	3.55e-15	1.78e-15

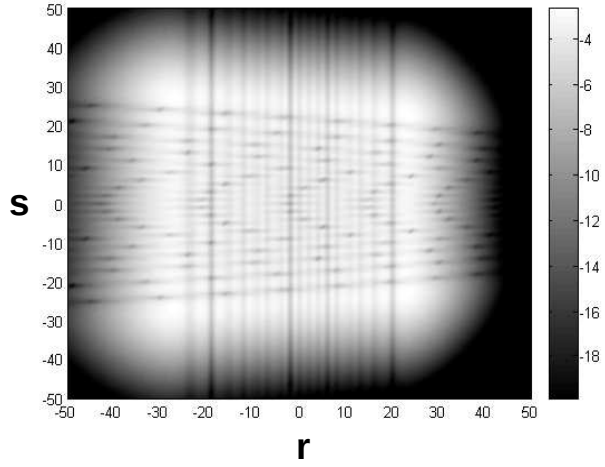

Figure 5. Plot of calculated energy distribution ($\log_{10}(e_{r,s})$) at order 10 for the example in Table 8.

the oscillatory integrals that enter a potential theoretic formulation of the scattering problem. We have shown that this high-order treatment can provide significant improvements over alternative low-order approximation procedures (e.g. the Kirchhoff approximation) throughout a broad spectrum at a modest additional computational cost. Results with full double precision accuracy were presented for a variety of configurations up to the resonance regime. As with other approximate high-frequency techniques, the current implementation of the method is restricted to non-shadowing configurations. Extensions to shadowing geometrical arrangements and to the full vector electromagnetic case will be the subject of future work.

Acknowledgments

Fernando Reitich gratefully acknowledges support from AFOSR through contract No. F49620-02-1-0052, from NSF through grant No. DMS–0311763, and from the Army High Performance Computing Research Center (AHPCRC) under Army Research Laboratory cooperative agreement number DAAD19-01-2-0014.

Disclaimer. Effort sponsored by the Air Force Office of Scientific Research, Air Force Materials Command, USAF, under grant number F49620-02-1-0052, and by AHPCRC under the auspices of the Department of the Army, Army Research Laboratory cooperative agreement number DAAD19-01-2-0014. The US Government is authorized to reproduce and distribute reprints for governmental purposes notwithstanding any copyright notation thereon. The views and conclusions contained herein are those of the author and should not be interpreted as necessarily representing the official policies or endorsements, either expressed or implied, of the Air Force Office of Scientific Research, the Army Research Laboratory or the US Government.

References

[1] Tsang L, Kong J A and R.T.Shin R T 1985 *Theory of Microwave Remote Sensing* (New York: Wiley)
[2] Brekhovskikh L M and Lysanov Y P. 1982 *Fundamentals of Ocean Acoustics* (Berlin: Springer-Verlag)
[3] Gaponov S V, Genkin V M, Salashchenko N N and Fraerman A A 1985 Scattering of neutrons and x radiation in the range 10–300Åby periodic structures with rough boundaries *JETP Lett.* **41** 63–65
[4] Reitich F and Tamma K K 2004 State-of-the-art, trends, and directions in computational electromagnetics *CMES* **5** 287–94
[5] Sei A, Bruno O P and Caponi M 1999 Study of polarization scattering anomalies with application to oceanic scattering *Radio Sci.* **34** 385–411
[6] Beckmann P and Spizzichino A 1963 *The Scattering of Electromagnetic Waves from Rough Surfaces: Part I. Theory* (London: Pergamon)
[7] Ulaby F T, Moore R K and Fung A K 1982 *Microwave Remote Sensing* vol II (Reading, MA: Addison-Wesley)
[8] Ulaby F T and Elachi C 1990 *Radar Polarimetry for Geoscience Application* (Boston, MA: Artech House)
[9] Ogilvy J A 1991 *Theory of Wave Scattering from Random Rough Surfaces* (Bristol: Adam Hilger)
[10] Lynch P J 1970 Curvature corrections to rough-surface scattering at high frequencies *J. Acoust. Soc. Am.* **47** 804–815
[11] Liszka E G and McCoy J J 1982 Scattering at a rough boundary —Extensions of the Kirchhoff approximation *J. Acoust. Soc. Am.* **71** 1093–1100
[12] Chaloupka H and Meckelburg H J 1985 Improved high-frequency current approximation for curved conducting surfaces *Arch. Elektron. bertragungstech.* **39** 245–250
[13] Rodriguez E 1989 Beyond the Kirchhoff approximation *Radio Sci.* **24** 681–693
[14] Bruno O, Sei A and Caponi M 2002 High-order high-frequency solutions of rough surface scattering problems *Radio Sci.* **37** 2/1-2/13
[15] Bruce N C 2004 On the validity of the inclusion of geometrical shadowing functions in the multiple-scatter Kirchhoff approximation *Waves Random Media* **14** 1–12

[16] Bouche D, Molinet F and Mittra R 1997 *Asymptotic Methods in Electromagnetics* (New York: Springer-Verlag)

[17] Bruno O P, Geuzaine C A, Monroe J A and Reitich F 2004 Prescribed error tolerances within fixed computational times for scattering problems of arbitrarily high frequency: the convex case *Phil. Trans. Roy. Soc. London* **362** 629–45

[18] Petit R. 1980 A tutorial introduction *Electromagnetic Theory of Gratings* (New York: Springer-Verlag) 1–40

[19] Chandler-Wilde S N and Zhang B 1998 Electromagnetic scattering by an inhomogeneous conducting or dielectric layer on a perfectly conducting plate *Proc. Royal Soc. London Ser. A* **454** 519–42

[20] Maue A W 1949 On the formulation of a general scattering problem by means of an integral equation *Z. Phys.* **125** 601-18

[21] Chen J S and Ishimaru A 1990 Numerical simulation of the second-order Kirchhoff approximation from very rough surfaces and a study of backscattering enhancement *J. Acoust. Soc. Am.* **88** 1846–50

[22] Melrose R and Taylor M 1985 Near peak scattering and the correct Kirchhoff approximation for a convex obstacle *Adv. in Math.* **55** 242–315

[23] Cullen J A 1958 Surface currents induced by short-wavelength radiation, *Phys. Rev. B* **109**, 1863–1867

[24] Fock V 1965 *Electromagnetic Diffraction and Propagation Problems* (London: Pergamon Press)

[25] Voronovich A G 1994 *Wave Scattering from Rough Surfaces* (New York: Springer-Verlag)

[26] Charnotskii M I and Tatarskii V I 1995 Tilt-invariant theory of rough-surface scattering: I *Waves Random Media* **5** 361–380

[27] Bleistein N and Handelsman R A 1986 *Asymptotic Expansions of Integrals* (New York: Dover)

[28] Bruno O P and Reitich F 1993 Numerical solution of diffraction problems: a method of variation of boundaries *J. Opt. Soc. Amer. A* **10** 1168–1175; *ibid* II. Dielectric gratings, Padé approximants and singularities 2307–2316; *ibid* III. Doubly periodic gratings 2551–2562